Sensitivity of a Cloud-Resolving Model to the Bulk and Explicit Bin Microphysical Schemes. Part I: Validations with a PRE-STORM Case

Xiaowen Li[1], Wei-Kuo Tao[2], Alexander P. Khain[3], Joanne Simpson[2], and Daniel E. Johnson[1]

[1]Goddard Earth Science and Technology Center
University of Maryland, Baltimore County
Baltimore, MD, USA

[2]Laboratory for Atmosphere
NASA Goddard Space Flight Center
Greenbelt, MD, USA

[3]The Hebrew University of Jerusalem
Jerusalem, Israel

Submitted to Journal of the Atmospheric Sciences

June, 2004

Abstract

A cloud-resolving model is used to study sensitivities of two different microphysical schemes, one is the bulk type, and the other is an explicit bin scheme, in simulating a mid-latitude squall line case (PRE-STORM, June 10-11, 1985). Simulations using different microphysical schemes are compared with each other and also with the observations. Both the bulk and bin models reproduce the general features during the developing and mature stage of the system. The leading convective zone, the trailing stratiform region, the horizontal wind flow patterns, pressure perturbation associated with the storm dynamics, and the cool pool in front of the system all agree well with the observations. Both the observations and the bulk scheme simulation serve as validations for the newly incorporated bin scheme. However, it is also shown that the bulk and bin simulations have distinct differences, most notably in the stratiform region. Weak convective cells exist in the stratiform region in the bulk simulation, but not in the bin simulation. These weak convective cells in the stratiform region are remnants of the previous stronger convections at the leading edge of the system. The bin simulation, on the other hand, has a horizontally homogeneous stratiform cloud structure, which agrees better with the observations. Preliminary examinations of the downdraft core strength, the potential temperature perturbation, and the evaporative cooling rate show that the differences between the bulk and bin models are due mainly to the stronger low-level evaporative cooling in convective zone simulated in the bulk model. Further quantitative analysis and sensitivity tests for this case using both the bulk and bin models will be presented in a companion paper.

1. Introduction

Cloud-resolving models have contributed significantly towards the understanding of cloud systems over the past four decades. With rapid advances in computer power, increasingly more advanced physical processes (e.g., surface flux, radiation, turbulent mixing, and topography) and numerical methods (e.g., grid nesting, positive definite schemes for scalar variables) have been incorporated into cloud-resolving models. These improvements, together with finer spatial resolution, longer integration time, larger model domain and more realistic initialization and large scale forcing, enable progressively better replications of the cloud/precipitation processes in cloud-resolving models. Although microphysical schemes in cloud-resolving models have improved greatly over time, the majority of current cloud-resolving models still use 'bulk' microphysical parameterizations, which is essentially the same as the Kessler (1969) scheme. A bulk scheme solves prognostic equations for mixing ratio of each hydrometeor type. It is conceptually simple and computationally efficient. However, bulk schemes cannot address questions related to variations of hydrometeor particle size and number concentration (e.g., modification of cloud properties and precipitation process by different aerosol concentrations.) 'Two-moment' schemes have been developed (e.g., Cotton et al. 1986; Murakami 1990; Wang and Chang 1993; Ferrier 1994; Meyers et al. 1997; and Carrió and Nicolini 2002) to represent cloud microphysics more realistically. 'Two-moment' schemes predict particle number concentrations in addition to their mixing ratios. However, this type of scheme still has to make crucial assumptions about initial drop concentrations, shapes of particle drop size distributions, and mean terminal fall velocities.

'Bin', or 'spectral bin' schemes, have been widely used in theoretical microphysics studies. They were also the natural choice in many early cloud models, whose dynamics were relatively simple and whose simulations did not involve any ice phase microphysics (e.g., Clark 1973; Soong 1974; Takahashi 1975). A bin scheme uses dozens, even hundreds of particle size bins to represent the drop size distribution of each hydrometeor type explicitly. Although more realistic compared with both bulk and two-moment schemes, bin schemes are computationally expensive and involve many uncertainties associated with detailed microphysical processes. Because of the complexity of bin schemes, together with the constraint of computer power, the success of the bulk type scheme in reproducing cloud dynamics in numerical models, and the shrinking funding toward basic research on cloud microphysics, the development of bin schemes in cloud-resolving models has been rather slow. A handful of bin schemes with both water and ice phase microphysics has been incorporated into cloud models (e.g., Hall 1980; Reisin et al. 1996; Khain and Sednev 1996; Ovtchinnikov and Kogan 2000). Hall (1980) incorporated a bin scheme to a 2-D slab model to simulate the impact of initial Cloud Condensation Nuclei (CCN) concentration on precipitation processes in a single convection. The model developed by Reisin et al. (1996) has been applied recently to the study of weather modification (e.g., Yin et al. 2000a) and the effects of giant CCN on convective cloud development. (Yin et al. 2000b). Ovtchinnikov et al. (2000) used their 3-D bin scheme cloud model to study ice production mechanisms in a small cumulus in New Mexico. Khain et al. (1999) used a 2-D cloud model with a bin microphysical scheme to study cloud-aerosol interaction in rain events in the Mediterranean.

A crucial question for cloud-resolving models using bin schemes is how it differs from the widely used bulk schemes. How do different microphysical schemes interact with

cloud and precipitation dynamics? In the early stages of cloud-resolving model development, Soong (1974) and Shiino (1983) used axisymmetric models to study the sensitivity of their models to bulk and bin schemes. Their models have warm rain microphysics only. They found that using different microphysical schemes resulted in significantly different cloud structures, cloud dynamics, and rain efficiencies. Soong (1974) also pointed out that even by varying the parameters, their bulk scheme could reproduce only certain features simulated by the bin scheme. Thus the bulk scheme could not substitute for the bin scheme by tuning its parameters, even for the relatively simple warm rain process in his case.

This paper presents a detailed comparison between bulk and bin microphysical schemes with both warm rain and ice microphsyics. The improved version of bin microphysical scheme in Hebrew University Cloud Model (HUCM) (Khain and Sednev 1996) is incorporated into the Goddard Cumulus Ensemble (GCE) model to study the sensitivity of a cloud-resolving model to different microphysical schemes. Another goal of this paper is to validate the newly incorporated bin scheme in the GCE model, with both previously available bulk scheme simulations and observations of a continental Mesoscale Convective System (MCS). In the next section, a brief description of both the GCE model and the HUCM bin microphysical scheme is given, together with a general description of June 10-11 PRE-STORM (the Preliminary Regional Experiment for Storm-scale Operational and Research Meteorology) case simulated in this paper. Detailed comparisons of both model simulations and observations are presented in section 3. The emphasis in section 3 is to identify major differences between the bulk and bin scheme simulations that can be directly compared to observations. Qualitative explanations of different model behaviors of the bulk and bin simulations are given in both section 3 and in a discussion in section 4. Further substantiation

of the theory in section 4 will be presented in a companion paper through different sensitivity tests using both the bulk and bin schemes. Finally, a summary and conclusions are given in section 5.

2. Model and case descriptions

2.1 GCE Model

A 2-D version of the GCE model is used in this study due to computational limitations. Dynamics in the GCE model are anelastic. The subgrid-scale turbulence is based on Klemp and Wilhelmson (1978). The bulk scheme in GCE model includes cloud water, rain, ice, snow and hail as described in Lin et al. (1983). The selection of the microphysical variables and parameters in the bulk scheme are suitable for the strong continental convections. Both solar and infrared radiation parameterizations are included in the model (Tao et al. 1996). All scalar variables use forward time and a positive, definite advection scheme with a non-oscillatory option (Smolarkiewicz and Grabowski, 1990). More details on the GCE model can be found in Tao and Simpson (1993a) and Tao et al. (2003).

2.2 HUCM Bin Scheme

The bin microphysical scheme in the HUCM explicitly describes the size distributions of seven hydrometeor types: cloud/rain, three types of ice (plate, column and branch), snow, graupel, and hail/frozen drops, as well as CCN. Each type has 33 size bins. Nucleation of CCN, ice nucleation, diffusional growth (condensation, evaporation, deposition, and sublimation) of all hydrometeors, freezing of water drops, an explicit description of ice particle melting, drop-drop, drop-ice, and ice-ice collision/coalescence are represented in this

bin scheme. Details of the bin scheme can be found in Khain and Sednev (1996) and Khain et al. (2000).

2.3 Experiment Design

The June 10-11, 1985 PRE-STORM case was a very well documented midlatitude mesoscale squall line (e.g., Johnson and Hamilton 1988; Ruteledge et al. 1988). The GCE model was initialized with a single sounding taken ahead of the newly forming squall line. There are 33 stretched vertical levels, with a resolution of 240 m at the lowest level and 1250 m at the top. The horizontal grid number is 1024, with 1 km resolution for the center 872 points. The outer grids are stretched. The total integration time is 12 hours with a 6 s time step. A lower level cool pool is applied for the first 10 minutes to initialize the convection. A modified horizontal wind profile with lower level shears is also applied. Further details of the experiment design for bulk scheme simulation can be found in Tao et al. (1993b).

Bin microphysics simulation uses exactly the same model settings a sdescribed above. The only difference is in the microphysical scheme. The initial aerosol concentration and size distribution are those of a clean continental background, with a small size CCN tail and no large CCN above 0.4 μm. The CCN concentration at super saturation of 1% is 600 cm^{-3}.

3. Comparisons

The bulk and bin simulations show many similar features, especially in terms of the system development. In both simulations, rain produced by a deep convective cell reaches the surface within about 20 minutes. New convections are then regenerated in front of the old cell, and the whole system propagates forward. Stratiform rain starts to form to the rear of the leading edge by the end of the second hour for the bulk scheme and earlier for the bin scheme.

The stratiform region keeps expanding with the evolution of the system. Maximum stratiform rain area is achieved after 6 to 7 hours and the system becomes quasi-steady after that, with regenerating convections at the leading edge and lighter stratiform rain trailing. The system simulated by the bulk scheme moves faster compared with the bin scheme. The system development simulated with both the bulk and bin scheme agrees well with the PRE-STORM case observations, as well as the initial and mature stages of a typical continental MCS. In conclusion, the newly incorporated bin scheme in the GCE model captures the developing and mature stage of a PRE-STORM MCS realistically, similar to the simulation of the well-accepted bulk scheme. No dissipation stage is simulated in this case because of the constant environmental conditions in the model.

In the rest of this section, more detailed comparisons between the bulk and bin models and observations are presented with the emphasis on the sensitivities of the model to the different microphysical schemes. A direct comparison between model and observation is very difficult due to limitations in both numerical modeling and field observations. While efforts have been made in this paper to use observations to validate model performance, the results should be considered only qualitative.

3.1 Radar Reflectivity

Radar reflectivity in the bulk model is calculated using parameterization according to Rutledge and Hobbs (1984). In the bin model, it is explicitly calculated according to particles' size distributions and densities. Figure 1 shows the radar reflectivity pattern at the end of the 12-hour simulations for the bulk (fig. 1a) and bin (fig. 1b) models. Both figures have a leading convective edge and a large area of trailing stratiform rain, a signature feature of MCSs.

The most prominent difference between figures 1a and 1b is in their stratiform region. The bulk simulation generally has vertical structures throughout the stratiform region, reflecting remnants of consecutive convective cells moving away from the leading edge into the trailing stratiform region. At this specific time, a dissipating convective core is identifiable by a high radar reflectivity center in fig. 1a around 80 km (x=150 km) behind the leading edge of the system. The stratiform region in the bin simulation (fig. 1b) is relatively homogeneous in horizontal direction compared with the bulk simulation. The convection cells dissipate very quickly after they move away from the leading edge. No vertical cellular structure is visible in the stratiform region in fig. 1b. Although only one instant radar reflectivity pattern was plotted in fig. 1 for each case, the above-described feature is consistent in radar reflectivity pattern throughout the whole simulation.

Radar reflectivity observations of June 10-11 PRE-STORM case have been described in many papers (e.g., Smull and Houze 1987a,b; Rutledge et al. 1988; Biggerstaff and Houze 1993). Figure 2 is taken from Rutledge et al. (1988). It shows one RHI scan during the mature stage of the June 10-11 PRE-STORM MCS. The leading convective zone and the large trailing stratiform region shown in fig. 2 qualitatively agree with modeled radar reflectivity pattern in both figures 1a and 1b. However, the horizontally homogeneous stratiform region simulated by the bin model compares better with the observation than the bulk model. In the bulk simulation, weak convective cells are identifiable well into the stratiform region, as shown in fig. 1a at x=150 km and x=180 km. Convective cells inside stratiform region have not been observed in June 10-11 PRESTORM case (e.g. Rutledge et al. 1988; Rutledge and MacGorman 1988; Biggerstaff and Houze 1993). As a matter of fact, Rutledge et al. (1988) described in their paper how the CP-4 radar was placed into a vertical mode right after the

passage of the convective line in order to specifically "determine the presence of convective-scale variations in the stratiform region that might result from generating cells". No such feature was reported in the June 10-11 PRE-STORM case. Convective cells embedded aloft in the stratiform region have been observed in other systems, e.g., Hobbs and Locatelli (1978), Businger and Hobbs (1987). To what extent they exist in continental MCSs is not clear. In this particular PRE-STORM case, there is no observational evidence supporting the existence of convective cells embedded in the stratiform region.

Differences in radar reflectivity patterns also exist in the leading convective zone when different microphysical schemes are used. In the bulk simulation, the height of the first convective cell is generally below 8 km in the mature stage. When the first cell reaches about 8 km, a new cell normally forms in front of it, cutting off its surface inflow. The original cell (now the second cell) continues to grow to above 12 km and usually is the tallest cell. In the bin model, the leading cell is always the tallest. New cells form close to the old cell, maintaining a strong updraft core at the leading edge which continuously progresses forward. Once the old cell leaves the leading updraft core, it quickly dissipates without further growth. Figure 3 shows time series of the height of the 30 dBZ echo top of the first convective cell for both the bulk (solid line) and bin (dotted line) simulations. In the early developing stage, both bulk and bin simulations have deep leading cells reaching above 10km. After the systems mature at around 350 minutes, the 30 dBZ radar echo top of the leading cell in the bulk simulation seldom exceeds 8km, whereas the bin model produces much higher echo tops. The radar observation in fig. 2 has its leading cell as the tallest, followed by a much weaker second cell. No radar pattern similar to fig. 1a has been found in the literature regarding the June 10-11 PRESTORM case. However, a shallow leading convective cell with taller second and third

cells similar to the bulk simulation in fig. 1a has been observed in other MCSs. (e.g., Chong et al. 1987). Again, bin scheme does a better job in replicating the radar reflectivity patters in the convective zone in this case study.

A prominent bright band exists in the observation in fig. 2, with its maximum reflectivity located around 3.5 km. The bin model successfully reproduces this feature, as shown in fig. 1b. The maximum reflectivity band is about 500m higher and has larger values than the observation in fig. 2 because of the simplification used in calculating radar reflectivities of mixed phase particles. It was simply assumed that the melting particles had a water coating so the refractive index for water was used for them. In reality, water rarely forms a coating around large particles. Instead the water is held in the ice interstices, forming a mixture of water, ice and air (Fujiyoshi 1986). According to the aircraft measurements of the same PRE-STORM system reported by Willis and Heymsfield (1989), the 0°C level in stratiform region was indeed around 4 km. Their study shows that a few large aggregates survived as ice to as warm as +5°C, which is another reason for the maximum bright band being below the 0°C level. The bulk model totally missed the bright band in the stratiform region despite the fact that the same simplification used in the bin model was used for bulk model calculations. Part of the reason is that the convective cells in the stratiform region in bulk simulation continuously transport water drops above the melting level, smearing out the melting signature in the radar reflectivity. Other possible reasons are: the coarse treatment of melting in the bulk microphysical scheme, and the fact that the bulk scheme has only high-density, fast-falling hail, whereas the bin scheme considers both hail and graupel. Falling snow contributes to the bright band in both bulk and bin simulations. However, its effect is relatively small because of its relatively low concentration in the stratiform region.

Several discrepancies exist for both bulk and bin simulations when compared with observations. For example, modeled radar reflectivities are higher than the observations in the convective region. The highest reflectivity measured in the leading convective core is about 50 dBZ, whereas the highest core reflectivities in both the bulk and bin simulations are all above 50dBZ. There are two possible reasons for the overestimation of radar reflectivity. First, the convection is too strong in numerical simulations. Since the direct measurement of vertical velocities in convective cores are very difficult, and indirect calculations (e.g., Rutledge and MacGorman, 1988) do not have enough resolution for the convective cells, this possibility remains an open issue. Second, the assumed particle size distribution could be too large in the bulk model. And the bin scheme could be producing excessive large particles. Since the bin microphysical scheme does not include raindrop breakup, this contributes at least partly to the higher radar reflectivities in the bin simulation. Another discrepancy with the observations is the lack of a transition zone near the surface between the convective and stratiform region in the models. A transition zone is a gap usually 10-30km wide with lowest radar reflectivity in the middle to lower atmosphere as shown in fig. 2 between –15 and –50 km. It has been widely observed in other squall-line systems. Biggerstaff and Houze (1993) analyzed the transition zone in the 10-11 June 1985 PRE-STORM system and concluded that the major contribution to its formation is the lack of small ice crystals in this zone caused by the downdrafts. Less aggregation leads to reduced rainfall in this region compared with the stratiform region. Further model development is needed in order to resolve this issue. Thirdly, the stratiform rain area in both models is relatively narrower compared with observations. The lack of stratiform rain exists in many other case studies using cloud-resolving models. This might be related to the lack of synoptic-scale forcing in the model settings.

3.2 Surface Rainfall

For 2-D simulations, time-domain contours as shown in fig. 4 provide a comprehensive picture of surface rainfall evolution. The bulk and bin schemes show very different surface rainfall patterns in fig. 4. The bulk model produces an oscillating surface rainfall with evidence of the rearward propagating convective cells clearly identifiable as high surface rainfall streaks. The bin scheme, on the other hand, shows a smooth surface rainfall pattern in fig. 4b. The leading convection merges quickly into the stratiform region with little evidence of rearward propagation in the surface rainfall. The trailing rain area in the bin simulation is larger than the bulk simulation. Instantaneous surface rainfall seldom exceeds 100 mm hr^{-1} in the bin simulation, while the bulk scheme consistently shows areas of surface rainfall of more than 100 mm hr^{-1}. The slopes of the leading edge lines in fig. 4 indicate that the system simulated with the bulk scheme propagates faster than the bin simulation. There is a strip of light rain immediately ahead of the convective region in the bin simulation (the forward overhang of the light precipitation), whereas there is little forward overhang in the bulk simulation. The observed radar reflectivity in fig. 2a does show a small, light rain strip in front of the leading convective edge. Radar composites for the same case described in Biggerstaff and Houze (1993) and Smull and Houze (1987a) support the existence of a forward overhang in the June 10-11 PRESTORM case, too.

The anvil stratiform rain trailing the convective line in MCSs contributes significantly to both the total surface rainfall and the mesoscale dynamics (e.g. Houze 1993). Two methods (i.e., Johnson and Hamilton 1988 (JH_88), and Churchill and Houze 1984 (CH_84)) are used in this study to separate stratiform and convective rain. The JH-88 method is used as a direct comparison with their PRE-STORM observations. CH_84 is a more widely used separation

method and is listed for comparison. The results are shown in table 1. Johnson and Hamilton (1988)'s stratiform percentage was calculated using densely deployed 5-minute rain gauge data collected during the passage of June 10-11 PRE-STORM squall line. Convective rain is assigned when the rainfall rate is above 6 mm hr^{-1}. When it falls below 6 mm hr^{-1}, the rain is categorized as stratiform. The same 6 mm hr^{-1} threshold is applied to instantaneous rainfall rates sampled at 1-minute intervals in model simulations. Using the JH_88 method, the bin scheme produces twice as much stratiform rain as the bulk scheme. However, both the bulk and bin simulations underestimate the stratiform rain compared with Johnson and Hamilton (1988) observation. The CH_84 method results much larger stratiform rain ratios for both the bulk (16%) and bin (28%) simulations as shown in table 1.

Figure 5 shows time series of domain-averaged surface rainfall for both the bulk (black lines) and bin (gray lines) simulations. The upper two lines represent total rainfall rate; The lower two lines represent stratiform rain rate using the CH_84 separation method. The bulk scheme has a much larger temporal oscillation compared with the bin scheme, in both total and stratiform rain. The average rainfall rates in bin model are less than bulk simulation except for the last 1 hour when they become similar. Probability distributions of surface rainfall are illustrated in fig. 6 where the percentage of the total rain amount is sorted by rain rate bins. The bulk simulation produces a surface rain spectra that is relatively flat up until 60 mm hr^{-1}, whereas the bin scheme has a large peak at smaller rainfall rates (less than 30 mm hr^{-1}). The bulk scheme also has a higher tail of large rainfall rates compared with the bin scheme.

3.3 Kinematic Structure

The horizontal wind fields of MCSs have many common features as described in, e.g., Houze (1993). Figure 7 illustrates the instantaneous horizontal wind of the bulk (7a) and

bin (7b) schemes at the end of the 12 hour simulations relative to the MCS. Similar to many previous observations and simulations of MCSs (see fig. 2b for an example), a deep front to rear flow exists at mid to upper levels, fed by the strong outflow from convective cells at the leading edge. This upper level outflow is responsible for carrying small ice particles rearward into the stratiform region. Dominant at the low to mid levels is a rear to front flow maintained mainly by evaporative cooling and water loading (Smull and Houze 1987b; Zhang and Gao 1989). A near surface front to rear flow prevails below 1.5 km. Both the model simulations shown in fig. 7 have similar horizontal wind structures and magnitudes compared with the observation in fig. 2b.

Several differences exist between the models and the observation. The observed rear to front inflow originates higher (above 9 km) than both simulations (below 8 km). The observed rear inflow in fig. 2b has an obvious downward slope that is lacking in both of the simulations. In the bulk simulation, the rear inflow descends to the surface after it enters the convective region, but it lowers down only slightly and never touches the ground in the bin simulation. The lack of a realistic large-scale environment for the current cloud-resolving model may explain the lower origin of the rear to front flow in the simulations. Zhang and Gao (1989) successfully reproduced the observed rear inflow structure in 10-11 June PRE-STORM case using a nested grid mesoscale model. Sensitivity tests in their study showed that when evaporative cooling was turned off, the rear to front inflow still originated at about the same height. But it did not penetrate into the stratiform region. They argued that large-scale baroclinity was responsible for the higher origin and partly the strength of the rear to front inflow. The lowering of the rear to front flow near the convective region is related to the relative strength of the positive vorticity generated by the cool pool at the rear side of the

convective region, and the negative vorticity produced by the bouyancy-gradience of the rear propagating convective cells, according to Weisman (1992). The bin simulation produces stronger upper level negative vorticity and weaker lower level positive vorticity compared with the bulk simulations, resulting less lowering of the rear to front flow in the bin simulation. More quantitative discussions will be given in a companion paper.

The instantaneous vertical air velocity (w) fields shown in fig. 8 are decisively different between the bulk and bin simulations. The updraft cores, defined here as areas with w stronger than 1 ms^{-1}, are darkly shaded. The downdraft cores stronger than –1 m s^{-1} are lightly shaded. There are more updraft cores in the bulk simulation (8a) than in the bin simulation (8b). In the bulk simulation, small updraft cores extend as far as 80 km from the leading edge. These updraft cores are responsible for the convective cells in the stratiform region as shown in fig. 1a. The bin simulation, however, has fewer updraft cores, and they are all within 30 km of the leading edge. The structures of the updraft cores in the bulk and bin simulations are different, too. In the bin simulation in fig. 8b, a single updraft core at the leading edge extends from the surface up to 15 km, with a slight rearward tilt. The air accelerates continuously along the core and achieves a maximum velocity of more than 20 m s^{-1} at around 8 km. The leading updraft core in the bulk simulation is much shorter, reaching only about 8km. The maximum w in fig. 8a is about 18 m s^{-1} and is achieved at around 4 km. The second updraft core, which is aloft at x=225 km in figure 8a, extends to 15 km and is totally separated from the first core by a downdraft core. Without continuous inflow from the surface, the air in the second core gains less momentum compared with the single core structure in fig. 8b. This contributes to a smaller maximum vertical air velocity in the bulk simulations as shown in fig. 9, a time series of the maximum and minimum w in both the bulk (solid lines) and bin (dotted lines) simulations.

Although the maximum w is weaker in bulk simulation, its minimum w is stronger due to strong rain evaporation in the convective region compared with the bin simulation.

More comprehensive updraft core statistics during the 12-hour simulation, including the average updraft core size, mean vertical air velocity in the core ($\overline{w}$), and number of cores at both 2 km and 8 km, are listed in table 2. The bulk scheme produces more, and slightly larger updraft cores at both levels, again illustrating the backward propagation of the convective celss. At 8 km, the average core strength in the bin simulation is 7 ms^{-1}, compared to only 3.3 ms^{-1} in the bulk scheme. This is consistent with the higher position of the maximum w in the bin simulation as shown in fig. 8.

Both single and dual-doppler radar analyses of the June 10-11 PRE-STORM case have been performed to derive the vertical air velocities (e.g., Rutledge et al. 1988; Rutledge and MacGorman 1988; Biggerstaff and Houze 1993). Comparable to the simulated instantaneous w field in fig. 8 is a dual-doppler analysis shown in fig. 6 in Biggerstaff and Houze (1993). The leading convective cell in their radar observation extends to above 13 km with the maximum w of more than 14 ms^{-1} located at around 9 km. There is no discontinuity on the updraft core in their observations as shown in the bulk simulation in fig. 8a. These features, and the higher location of the maximum w, compare favorably with the bin simulation.

The downdraft cores exist at both upper and lower levels, as shown in fig. 8. Lower-level downdraft cores are driven mainly by evaporative cooling and water loading, and are of interest in this study. As shown in fig. 8, lower-level downdraft cores immediately adjacent the leading convection have very different strengths and sizes in the bulk and bin simulations. The bulk simulation in fig. 8a shows an intense downdraft core of more than -5 m s^{-1} located at x=225 km. In the bin model, the downdraft core at around x=198 km in fig. 8b has a maximum

strength of only -2 ms^{-1}. This downdraft core is not only weaker in strength, but also smaller in size compared with bulk simulation. This is consistent with the minimum w time series shown in fig. 9, where time series of the minimum w below 5 km are plotted. These minimum w represents the strongest lower level downdraft which normally occurs right behind the leading convection. The downdrafts in the bulk model are always stronger, and have larger temporal variations compared with the bin simulation. The reason is that in the bulk scheme, a large amount of rain falls into the downdraft region due to the backward tilting of the first cell and the formation of a second updraft core directly above the downdraft core. More evaporation results in the bulk model compared with the more upright, continuous convective core simulated in the bin model. The majority of the rain in the bin model falls within the leading updraft core, resulting in a much smaller and less intense downdraft core immediately behind the leading line.

Vertical air velocity structures in the stratiform region shown in fig. 8 are very different too. The bin simulation has a nearly continuous weak updraft above 7km and downdraft below it. The bulk simulation shows alternating updraft and downdraft in the stratiform region, similar to its convective region, but with much weaker strengths and lower frequencies.

The previous observations have been focused on the domain-average vertical velocity profiles in the stratiform region in MCSs, which show a very consistent pattern of weak updraft/downdraft at upper/lower levels (see Houze, 1993 for a comprehensive review). In order to compare model simulations with the observations, the simulated w profiles in the stratiform region are plotted in fig. 10 using non-solid lines. These are the instantaneous domain-average profiles at t=12 hours. In the bulk simulation, there are alternating updrafts

and downdrafts in stratiform region. Therefore the shapes of the domain-average profiles are very sensitive to the size and location of the domain specified. For example, starting from the first grid at the rear of the system where surface reflectivity is larger than 0 dBZ (x~150 in fig. 1), different domain sizes are used to calculate the average profile for the bulk scheme. The dashed line in fig. 10 is the average from x=150 to x=190 (40 km domain), and the dash-dot line is the average from x=150 to x=210 (60 km domain). The average w at lower levels is positive over the 40 km domain in the bulk case, which is contrary to all the observations. However, when w are averaged over the 60 km domain, the profile becomes negative at lower levels, because the large downdraft core at around x=200 km in fig. 10 is now included in the calculation.

For the June 10-11 PRE-STORM case, average w profiles in the stratiform region have been reported in Rutledge et al. (1988) using single doppler radar EVAD measurements, and in Biggerstaff and Houze (1993) using dual-doppler radar analysis. Their results are reproduced in fig. 10 in solid lines. The three observations agree with each other qualitatively, but not quantitatively. The general structure and magnitude of the average updraft/downdraft in both bin simulation and bulk simulation using 60 km domain average agree qualitatively with observations. But discrepancies do exist. Both CP3 and dual-doppler observations show a maximum downdraft near the melting level. CP4 has a lower maximum downdraft. The w profile in the bulk simulation for the 60 km domain has its maximum near the melting level. The bin simulation produces a downdraft peak about 1.2 km above the melting level. This indicates that significant sublimation occurs in the bin simulation above the melting level.

3.4 Pressure

Pressure perturbation fields at t=12 hours are plotted in fig. 11 Both the bulk and bin models are able to capture some of the common features observed in the June 10-11 PRESTORM case. For example, a surface high-pressure center generated by the cool gust front coincides with the arrival of strong convective rain for both bulk and bin simulations. This agrees with the surface pressure observation described in Johnson and Hamilton (1988), where in a single surface station, a pressure jump of 4 mb was observed, followed by heavy rain within five minutes. The surface pressure jump in the bulk simulation is 2.2 mb, and it is 3.3 mb in the bin simulation. The bin simulation in fig. 11b shows a small pre-squall low at x=220 km. A pre-squall low is reported in Johnson and Hamilton (1988) in their figure 13. The bulk simulation does not have a pre-squall low center, nor is the pre-squall low a persistent feature in the bin simulations. Both models show a meso-low with similar intensity at mid-levels of the MCSs. This feature is consistent with the pressure perturbation field retrieved from the doppler radar observations of the June 10-11 PRE-STORM case (Braun and Houze, 1994). Multiple low centers exist in the bulk simulation (at x=190 km and 160 km) but not in the bin simulation, presumably because of the multiple convective cells in bulk model. Neither the bulk nor the bin model can reproduce the surface meso-low center to the rear of the system, which was observed by Johnson and Hamilton (1988) and simulated by Zhang and Gao (1989). This surface rear low is believed to be induced by the heating of the middle to low level downdraft, which is also missing in the simulations, as shown in fig. 8. This may be part of the reason for the lack of downward tilt in the mid-level rear to front flow as shown in fig. 7. Generally, the cloud-resolving model can not reproduce pressure perturbation features associated with large-scale dynamics, for example, the surface wake-low. However, both the

bulk and bin schemes successfully simulated pressure features generated by local dynamics, such as the surface high before the leading edge and the mid-level meso-low center.

3.5 Thermodynamical and microphysical fields

In the previous sections, the radar reflectivity, surface rainfall, wind, and pressure field simulated by both the bulk and bin models have been compared, with the emphasis on the differences between the two microphysical schemes. These simulations were also compared with the applicable observations. The instantaneous fields presented in previous sections are representative of the later, quasi-steady stage (the last 6 hours) of the simulated storm. Time-average plots tend to obscure features like the cellular structure of the vertical air velocity in the bulk scheme when comparing with the observations. Although both the bulk and bin models are able to reproduce many important features observed in the June 10-11 PRE-STORM case, distinct differences exist between them. This shows the important role the microphysical scheme plays in the cloud-resolving model. In the following sections, mechanisms that produce the differences between the bulk and bin simulations will be investigated by analyzing thermodynamical and microphysical outputs from the models.

Figure 12 shows the instantaneous potential temperature perturbation at t=12 hours. –3 K contour level is highlighted with thick dashed lines. Again the bulk and bin simulations show distinct differences. The diabatic heating in the convective region is more organized in the bin model (12b) due to its deeper and more organized updraft cores than the bulk model (12a). The negative potential temperature perturbation at lower levels in the bin simulation is deeper but less intense compared with the bulk simulation. In the bulk simulation, negative potential temperature is mainly confined below 3 km in the rear part of the system, with a thick head coinciding with the leading convection edge. This structure is similar to a density current

and has also been described in other cloud-resolving models (e.g., Fovell and Ogura 1988). The minimum temperature is below –5 K in the cold head. The bin simulation has negative potential temperature extending up to 5 km. A cool pool with a minimum potential temperature of less than –4 K exists at the leading convection edge. However, the cool air does not spread to the ground as the bulk model does. The potential temperature perturbation near the ground in the rear part of the system is much warmer in the bin simulation (~-1K) than in the bulk simulation (~-4K). Several factors may contribute to these differences. First, the rear to front inflow in bulk model (fig. 7a) lowers to the ground near the leading edge, cutting off the near surface front to rear flow. Warmer, unperturbed air in front of the system cannot reach the rear of the system directly. Surface air at the rear part of the system comes mainly from evaporatively cooled air from strong downdrafts in the convective zone. The bin model, however, has a continuous front to rear near surface flow (fig. 7b). Some of the near surface air at the rear of the system comes directly from the warm surface air in front of the system, resulting to a warmer near surface potential temperature compared with the bulk model. Secondly, evaporative cooling in the convective region, the major source of the cold air near the ground, is much stronger in the bulk simulation. This can be inferred from the stronger, broader downdraft cores in the convective region shown in fig. 8a. Third, sublimation above the melting level is stronger in the bin simulation as inferred from both fig. 9 and fig. 10. This contributes to the cooler air at middle levels and thus a thicker negative region in the bin simulation. The potential temperature perturbation retrieval by Braun and Houze (1994) showed a density current type of structure with the coolest air near the surface, similar to the bulk simulation. More quantitatively comparison is difficult due to the assumptions and limited resolutions in the retrieval.

Direct evidence that evaporative cooling in the convective region is stronger in the bulk simulation is shown in fig. 13, where the condensation/evaporation rate contours in units of g g^{-1} day^{-1} at t=12 hours are plotted. Condensation is shown in solid lines and evaporation in dashed lines. Areas with evaporation rates stronger than –0.1 g g^{-1} day^{-1} are shaded with gray. Patches of condensation/evaporation occur in the upper stratiform region in the bulk simulation but not in the bin simulation. This is consistent with the existence of updraft cores in stratiform region in fig. 8. Evaporation in the stratiform region is much stronger in the bin simulation as shown by the size of the shaded area in the stratiform regions. The maximum evaporation rate there is stronger than –0.2 g g^{-1} day^{-1} in the bin simulation, compared with just –0.1 g g^{-1} day^{-1} in the bulk simulation. This contributes to the stronger average downdraft in the stratiform region in the bin simulation as shown in fig. 10.

Contrary to the stratiform region evaporation described above, evaporation in the convective zone in the bulk simulation (shaded between x=220 and 230 km in fig. 13a) is much broader compared with the bin simulation (shaded at around x=200 km in fig. 13b). The magnitude of the evaporation rate is similar for both models at this time. However, average evaporation in the convective region is stronger in the bulk simulation as shown in fig. 14, where time series of the strongest evaporation rate below the melting level for the bulk (solid line) and bin (dotted line) model are shown. During the quasi-steady state toward the later half of the simulation, deep spikes of strongest evaporation rate happens in the bulk simulation, but they are much weaker in the bin simulation. These spikes may cause the bore like structures in the potential temperature perturbation shown in fig. 12a. For example, local potential temperature minimum can be identified at x=220 km, x=190 km, x=160 km and x=135 km in

figure 12a. Th bin model has relatively less temporal variations in the maximum evaporation rate compared with bulk model during the latter half of the simulation.

4. Discussion

Both the bulk and bin microphysical models are able to successfully reproduce general features observed in the June 10-11 PRE-STORM case. However, the model simulations are very sensitive to different microphysical schemes. With identical model setup, initial, and environmental conditions in the GCE model, two self-consistent microphysical schemes produce very different details in the storm structure as discussed in the previous sections. This indicates the importance of the microphysical scheme in the cloud-resolving model. In this section, some general discussions to explain the model sensitivity to different microphysical schemes are given. Further analysis and substantiation of these points will be presented in a companion paper using sensitivity tests with both the bulk and bin models.

Diabatic heating/cooling is the key to cloud microphysics-dynamics interaction. In this particular case study, different patterns and strengths of the evaporative cooling produced by different microphysical schemes are largely responsible for their different structures. In the convective region, the bulk scheme has stronger and broader evaporative cooling (fig. 13 and 14) during the mature stage of the system. This produces a stronger downdraft core (fig. 8) and near surface cool pool (fig. 13) in the bulk model correspondingly. The near surface cool pool, coupled with environmental wind shear and the strength of the rear to front inflow, is responsible for the regeneration of new convective cells at the front of the system and the sustaining of a forward moving, long-lasting squall line (e.g., Rotunno et al. 1988; Morris and Rotunno 2004). The stronger cool pool (fig. 13) and downdraft (fig. 8) in the bulk scheme produce a faster moving system compared with the bin simulation (figure 4). With the same

environmental wind shear, the stronger cool pool in bulk simulation forms a situation similar to the "less-than-optimal shear, but a long-lived state" in Rotunno et al. (1988). This type of system is slanted upshear, as evident in the multiple cells in fig. 1a. The instantaneous vertical velocity in the bulk simulation (fig. 8a) suggests that the slanted updraft core is cut off by a deep downdraft core, generated by both evaporative cooling at lower levels and mechanical forcing at upper levels. The residual updraft core moves continuously toward the rear of the system while maintaining some of its buoyancy. This forms multiple convective cells extending far behind convective line into the stratiform region. The bin simulation, on the other hand, has a weaker cool pool and a more upright convective core at the leading edge. The majority of its rain falls within its updraft core, resulting in less evaporation and a weaker cool pool. The more upright leading convective core keeps the buoyant air within itself, forming a stronger and tall updraft core, and larger maximum air velocity in the bin simulation (fig. 9). When the air leaves the leading updraft core at the upper levels, it quickly loses its buoyancy and forms the stratiform region. The majority of the stratiform rain in the bin simulation comes from the ice particles transported rearward by the upper level flow. On the other hand, portion of stratiform rain in the bulk simulation still come from the condensation/deposition within the residual updraft cores. More quantitative analysis will be discussed in a companion paper.

4. Summary and future work

The GCE model coupled with the HUCM explicit microphysical bin scheme is used to simulate the June 10-11 PRE-STORM MCS. Simulations using both the bulk and the newly incorporated bin microphysical scheme have successfully reproduced many features observed in this case (e.g., the evolution of the system to the mature stage, the distribution of the convective and stratiform rain, the horizontal flow structure, and the storm induced pressure

perturbation patterns). These results serve as a validation for the robustness of the bin scheme in the long-term simulations of continental MCSs. However, the modeled cloud dynamics also exhibit sensitivities to the different microphysical schemes, as evident in the many differences between the bulk and bin models detailed in this paper. The most prominent difference occurs in the stratiform region. In the bulk simulation, convective cell structures extend well into the stratiform region, whereas the bin simulation shows a horizontally homogeneous stratiform rain. The simulated radar reflectivity, surface rainfall, and vertical air velocity all bear signatures of convective cells in stratiform region in the bulk simulation. Radar observations of the same case do not show convective cellular structures in the stratiform region. The bin scheme is superior to the bulk scheme in reproducing a homogeneous stratiform rain in this PRE-STORM case.

The reasons for the differences between the bulk and bin simulations are also discussed briefly. The bulk scheme produces stronger evaporative cooling in the convective region compared with the bin model. The resulted strong surface cool pool in the bulk simulation interacts with low-level wind shear in front of the system to form slanted convective cells. These cells are cut off by downdraft cores immediately behind the leading convection. Remnant cells carry enough momentum and buoyancy to survive well into the stratiform region. The bin simulation, on the other hand, has a weaker cool pool and more upright convective cells. The convective cells quickly lose their buoyancy after they leave the leading edge and merge into the stratiform region, forming a more homogeneous stratiform rain.

There are features that are missed by both bulk and bin simulations, notably the lack of a transition zone between the convective and stratiform region, and the low origin and the lack of the downward bending of the rear to front inflow. It is hoped that finer vertical and

horizontal resolution in the cloud-resolving model, and more realistic representation of the particle falling velocity could improve the representation of the transition zone in a continental MCS. The lack of a realistic large scale influence in the current GCE model is believed to be responsible for missing the downward bending of the rear to front inflow.

Simulations of the June 10-11 PRE-STORM MCS show that both the bulk and bin model can reproduce the general structure of the developing and mature stage of the system. However, when compared with details in observations, both models are able to capture some, but not all of the features. The more sophisticated bin scheme shows superiority over the bulk model in reproducing some of the MCS structures. It also have a large potential in studying the cloud-aerosol interaction and its impact on the cloud dynamics and precipitation processes, which can not be achieved using a bulk scheme. Although not attempted in this paper, the bin scheme adds more opportunities in the direct comparison between the model and the observations, especially with the detailed microphysical measurements. Furthermore, there will be less constraint in terms of particle size distribution specification when the cloud-resolving model results are used to interpret and retrieve remote sensing (e.g., radar, microwave) data.

Acknowledgments: This research is mainly supported by the NASA headquarters and the NASA TRMM Mission. The authors are grateful to Dr. R. Kakar at NASA headquarters for his support of this research. Acknowledgement is also made to the NASA/GSFC for computer time used in this research.

References:

Biggerstaff, M. I., and R. A. Houze, Jr., 1993: Kinematics and microphysics of the transition zone of the 10-11 June 1985 squall line. *J. Atmos. Sci,* **50,** 3091-3110.

Braun, S. A. and R. A. Houze, Jr., 1994: The transition zone and secondary maximum of radar reflectivity behind a midlatitude squall line: Results retrieved from doppler radar data. *J. Atmos. Sci.,* **51,** 2733-2755.

Businger, S., and P. V. Hobbs, 1987: Mesoscale structures of two comma cloud systems over the Pacific Ocean. *Mon. Wea. Rev.,* **115,** 1908-1928.

Carrió, G. G., and M. Nicolini, 2002: An alternative procedure to evaluate number concentration rates in two-moment bulk microphysical schemes. *Atmos. Res.,* **65,** 93-108.

Churchill, D. D., and R. A. Houze, Jr., 1984: Development and structure of winter monsoon cloud clusters on 10 December 1978. *J. Atmos. Sci.,* **41,** 933-960.

Clark, T. L., 1973: Numerical modeling of the dynamics and microphysics of warm cumulus convection. *J. Atmos. Sci.,* **30,** 857-878.

Cotton, W. R., G. J. Tripoli, R. M. Rauber and E. A. Muluihill, 1986: Numerical simulation of the effects of varying ice crystal nucleation rates and aggregation processes on orographic snowfall. *J. Climate Appl. Meteor.,* **25,** 1658-1680.

Ferrier, B. S., 1994: A double-moment multiple-phase four-class bulk ice scheme. Part I: Description. *J. Atmos. Sci.,* **51,** 249-280.

Fovell, R. G., and Y. Ogura, 1988: Numerical simulation of a midlatitude squall line in two dimensions. *J. Atmos. Sci.,* **45,** 3846-3879.

Fujiyoshi, Y., 1986: Melting snowflakes. *J. Atmos. Sci.,* **42,** 307-311.

Hall, W. D., 1980: A detailed microphysical model within a two-dimensional dynamical framework: Model description and preliminary results. *J. Atmos. Sci.,* **37,** 2486-2507.

Hobbs, P. V., and J. D. Locatelli, 1978: Rainbands, precipitation cores and generating cells in a cyclonic storm. *J. Atmos. Sci.,* **35,** 230-241.

Houze, R. A., Jr, 1993: Cloud dynamics. *Academic Press,* 573pp.

Johnson, R. H., and P. J. Hamilton, 1988: The relationship of surface pressure features to the precipitation and airflow structure of an intense midlatitude squall line. *Mon. Wea. Rev.*, **116,** 1444-1472.

Kessler, E., III, 1969: On the distribution and continuity of water substance in atmospheric circulation. *Meteor. Monogr.*, American Meteorological Society, pp84.

Khain, A. P., and I. Sednev, 1996: Simulation of coastal circulation in the Eastern Mediterranean using a spectral microphysics cloud ensemble model. *Atmos. Res.*, ***43,*** 77-110.

Khain, A. P., A. Pokrovsky, and I. Sednev, 1999: Some effects of cloud-aerosol interaction on cloud microphysics structure and precipitation formation: numerical experiments with a spectral microphysics cloud ensemble model. *Atmos. Res.*, **52,** 195-220.

Khain, A., M. Ovtchinnikov, M. Pinsky, A. Pokrovsky, and H. Krugliak, 2000: Notes on the state-of-the-art numerical modeling of cloud microphysics. *Atmos. Res.*, **55,** 159-224.

Klemp, J. B., and R. B. Wilhelmson, 1978: The simulation of three-dimensional convective storm dynamics. *J. Atmos. Sci.*, **35,** 1070-1096.

Lin, Y.-L., R. D. Farley, and H. D. Orville, 1983: Bulk parameterization of the snow field in a cloud model. *J. Climate Appl. Meteor.*, **22,** 1065-1092.

Meyers, M. P., R. L. Walko, J. Y. Harrington, and W. R. Cotton, 1997: New RAMS cloud microphysics parameterization. Part II: The two-moment scheme. *Atmos. Res.*, **45,** 3-39.

Morris, L. W. and R. Rotunno, 2004: "A theory for strong long-lived squall lines" revisited. *J. Atmos. Sci.*, **61,** 361-382.

Murakami, M., 1990: Numerical modeling of dynamical and microphysical evolution of an isolated convective cloud – The 19 July 1981 CCOPE cloud. *J. Meteor. Soc. Japan,* **68,** 107-128.

Ovtchinnikov, M., Y. L. Kogan, 2000: An investigation of ice production mechanisms in small cumuliform clouds using a 3D model with explicit microphysics. Part I: Model description. *J. Atmos. Sci.*, **57,** 2989-3003.

_____, Y. L. Kogan, and A. M. Blyth, 2000: An investigation of ice production mechanisms in small cumuliform clouds using a 3D model with explicit microphysics. Part II: Case study of New Mexico cumulus clouds. *J. Atmos. Sci.*, **57,** 3004-3020.

Reisin, T., Z. Levin, and S. Tzivion, 1996: Rain production in convective clouds as simulated in an axisymmetric model with detailed microphsyics. Part I: Description of the model. *J. Atmos. Sci.*, **53,** 497-519.

Rotunno, R., J. B. Klemp, and M. L. Weisman, 1988: A theory for strong, long-lived squall lines. *J. Atmos. Sci.*, **45**, 463-485.

Rutledge, S. A., and P. V. Hobbs, 1984: The mesoscale and microscale structure and organization of clouds and precipitation in midlatitude clouds. Part XII: A diagnostic modeling study of precipitation development in narrow cold frontal rainbands. *J. Atmos. Sci.*, **41**, 2949-2972.

Rutledge, S. A., R. A. Houze, Jr., and M. I. Biggerstaff, 1988: The Olkahoma-Kansas mesoscale convective system of 10-11 June 1985: Precipitation structure and single-doppler radar analysis. *Mon. Wea. Rev.*, **116**, 1409-1430.

Rutledge, S. A., and D. R. MacGorman, 1988: Cloud-to ground lightening activity in the 10-11 June 1985 mesoscale convective system observed during the Oklahoma-Kansas PRE-STORM project. *Mon. Wea. Rev.*, **116,** 1393-1408.

Shiino, J., 1983: Evolution of raindrops in an axisymmetric cumulus model. Part I. Comparison of the parameterized with non-parameterized microphysics. *J. Meteor. Soc. Japan,* **61,** 629-655.

Smolarkiewicz, P. K., and W. W. Grabowski, 1990: The multidimensional positive advection transport algorithm: nonoscillatory option. *J. Comput. Phys.*, **86,** 355-375.

Smull, B. F., and R. A. Houze, Jr., 1987a: Dual-Doppler radar analysis of a midlatitude squall line with a trailing region of stratiform rain. *J. Atmos. Sci.*, **44,** 2128-2147.

Smull, B. F., and R. A. Houze, Jr., 1987b: Rear inflow in squall lines with trailing stratiform precipitation. *Mon. Wea. Rev.*, **115,** 2869-2889.

Soong, S., 1974: Numerical simulation of warm rain development in an axisymmetric cloud model. *J. Atmos. Sci.*, **31,** 1262-1285.

Takahashi, T., 1975: Tropical showers in an axisymmetric cloud model. *J. Atmos. Sci.*, **32,** 1318-1330.

Tao, W.-K. and J. Simpson, 1993a: Goddard Cumulus Ensemble Model. Part I: Model description. *Terr. Atmos. Oceanic Sci.*, **4,** 35-72.

_____, J. Simpson, C.-H. Sui, B. Ferrier, S. Lang, J. Scala, M.-D. Chou, and K. Pickering, 1993b: Heating, moisture, and water budgets of tropical and midlatitude squall lines: Comparisons and sensitivity to longwave radiation. *J. Atmos. Sci.*, **50,** 673-690.

_____, S. Lang, J. Simpson, C.-H. Sui, B. Ferrier, and M.-D. Chou, 1996: Mechanisms of cloud-radiation interaction in the tropics and midlatitudes. *J. Atmos. Sci.*, **53,** 2624-2651.

_____, J. Simpson, D. Baker, S. Braun, M.-D. Chou, B. Ferrier, D. Johnson, A. Khain, S. Lang, B. Lynn, C.-L. Shie, D. Starr, C.-H. Sui, Y. Wang, and P. Wetzel, 2003: Microphysics, radiation and surface processes in the Goddard Cumulus Ensemble (GCE) model. *Meteorol. Atmos. Phys.*, **82,** 97-137, 2003.

Wang, C., and J. S. Chang, 1993: A three-dimensional numerical model of cloud dynamics, microphysics, and chemistry, 1, Concepts and formulation, *J. Geo. Res.*, **98(D8),** 14827-14844.

Weisman, M. L, 1992: The role of convectively generated rear-inflow jets in the evolution of long-lived mesoconvective systems. *J. Atmos. Sci.*, **49,** 1826-1846.

Willis, P. T. and A. J. Heymsfield, 1989: Structure of the melting layer in mesoscale convective system stratiform precipitation. *J. Atmos. Sci.,* **46,** 2008-2025.

Yin, Y., Z. Levin, T. G. Reisin, and S. Tzivion, 2000a: Seeding convective clouds with hygroscopic flares: Numerical simulations using a cloud model with detailed microphysics. *J. Appl. Meteorol.,* **39,** 1460-1472.

_____, _____, _____, and _____, 2000b: The effects of giant cloud condensation nuclei on the development of precipitation in convective clouds—A numerical study. *Atmos. Res.,* **53,** 91-116.

Zhang, D.-L., and K. Gao, 1989: Numerical simulation of an intense squall line during 10-11 June 1985 PRE-STORM. Part II: Rear inflow, surface pressure perturbations and stratiform precipitation. *Mon. Wea. Rev.,* **117,** 2067-2094.

Figure Captions:

Figure 1: Radar reflectivity after 12 hours of simulation for the bulk (1a) and bin (1b) schemes.

Figure 2: Radar reflectivity and horizontal relative flow in m s^{-1} observed at 0345 UTC in the June 10-11 PRE-STORM case. Copied from fig. 5 in Rutledge et al. (1988).

Figure 3: Time series of 30 dBZ radar echo top of the leading convective cell in the bulk (solid line) and bin (dashed line) simulations.

Figure 4: Time-domain diagram of surface rainfall for the bulk (4a) and bin (4b) schemes.

Figure 5: Time series of the domain average surface rainfall rate for the bulk (black lines) and bin (gray lines) simulations. The upper two lines are total surface rainfall rate, and lower two lines are stratiform rainrate using the CH_84 separation method.

Figure 6: Surface rainfall amount probability density plot for the June 10-11 PRE-STORM case.

Figure 7: Horizontal wind field at the end of the simulation (12 hours) for the bulk (7a) and bin (7b) scheme. Contour levels are -15, 10, -5, 0, 5, 10, and 15m s^{-1}, with negative contours shown in dashed lines.

Figure 8: Vertical air velocity field after 12 hours of simulation for the bulk (8a) and bin (8b) scheme. Contour levels are –5, –1, -0.5, -0.1, 0.1, 1, 5, 10, and 20 m s^{-1}, with negative contours shown in dashed lines. Updraft cores with w bigger than 1 m s^{-1} are darkly shaded. Downdraft cores with w less than –1 m s^{-1} are lightly shaded.

Figure 9: Time series of maximum and minimum vertical air velocity (m s^{-1}) for both the bulk (solid lines) and bin (dotted lines) simulations. Negative values represent downdrafts. The minimum velocity is calculated using only data below 5 km.

Figure 10: Average vertical air velocity profiles for the stratiform region 12 hours into the simulation. The dotted line is for the bin simulation averaged between x=130 km and 180 km in fig. 8b. The dashed line is for the bulk simulation averaged between x=150 km and 190 km in fig. 8a; The dashed-dot line is for the bulk simulation averaged between x=150 km and 210 km in fig. 8a. Thin solid lines are from EVAD calculations of the same case using CP3 and CP4 radar (Rutledge et al. 1988), and the thick solid line is the dual doppler radar estimation (Biggerstaff and Houze 1993).

Figure 11: Pressure perturbations in mb for both the bulk and bin simulations. Positive/negative values are in solid/dashed lines. The contour intervals are 0.5 mb.

Figure 12: Potential temperature perturbation fields at t=12 hours for the bulk (12a) and bin (12b) models. Contour levels are –5 –4, -3, -2, -1, 0, 2, 4, 6 K, with negative contours in dashed lines. –3 K lines are marked with thick dashed lines.

Figure 13: Condensation/evaporation rate field in g g^{-1} day^{-1} for the bulk (13a) and bin (13b) simulations. Positive values (condensation) are in solid lines, and negative values (evaporation) are in dashed lines. Contour levels are –0.2, -0.1, -0.05, -0.01, 0.01, 0.05, 0.1, 1.0 g g^{-1} day^{-1}. Areas with evaporation rates stronger than –0.1 g g^{-1} day^{-1} are shaded in gray.

Figure 14: Time series of the maximum evaporation rate in g g^{-1} day^{-1}. Only evaporation rates below the melting level are used. The solid (dashed) line is the bulk (bin) simulation.

Table Captions:

Table 1: Stratiform rain percentage for the June 10-11 PRESTORM case.

Table 2: Updraft core statistics for the PRE-STORM case.

Table 1: Stratiform rain percentage for the June 10-11 PRE-STORM case.

Case	Bulk	Bin
Ave. rainrate (mm/day)	47.4	32.8
Stratiform rain (JH_88)	5%	10%
Stratiform rain (CH_84)	16%	28%
Observation	29% (JH_88)	

Table 2: Updraft core statistics for the PRE-STORM case.

Case		Bulk	Bin
2 km	Core size (km)	4.6	3.9
	Core number	4.1	1.2
	$\overline{w}$ (ms^{-1})	3.1	3.4
8 km	Core size (km)	5.3	4.7
	Core number	5.4	2.3
	$\overline{w}$ (ms^{-1})	3.3	7.0

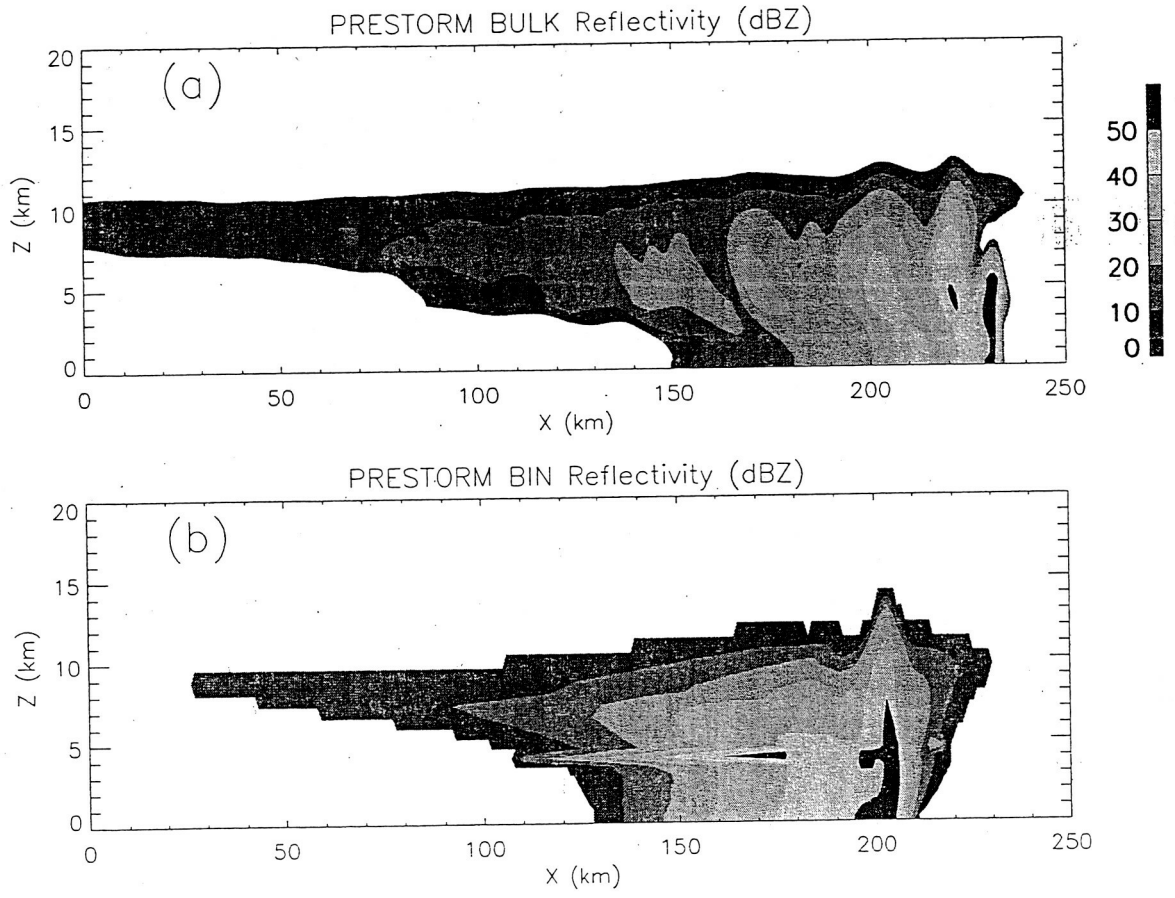

Figure 1: Radar reflectivity after 12 hours of simulation for the bulk (1a) and bin (1b) schemes.

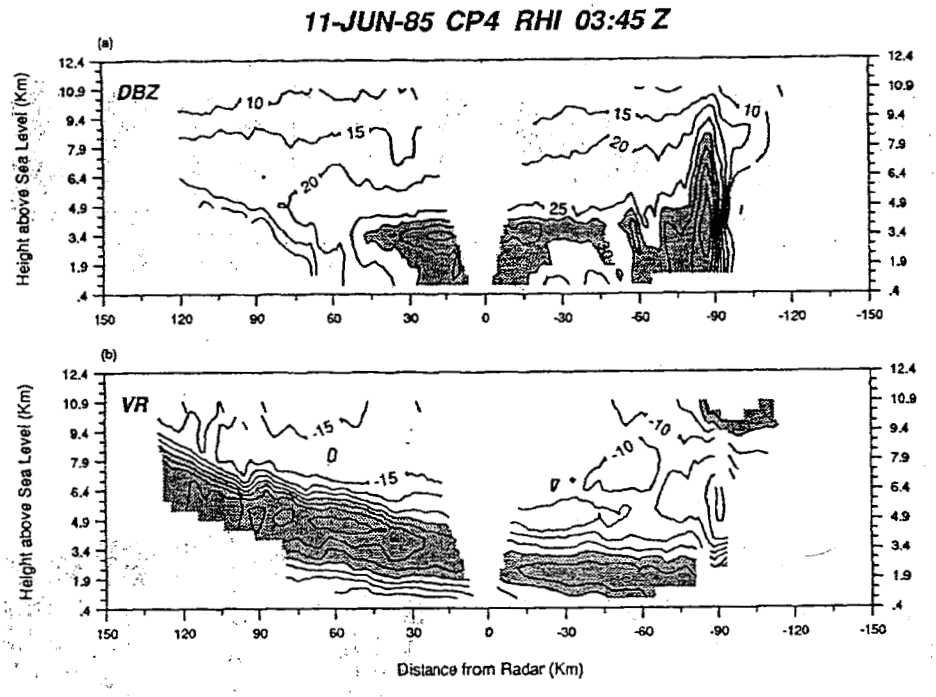

Figure 2: Radar reflectivity and horizontal relative flow in m s^{-1} observed at 0345 UTC in the June 10-11 PRE-STORM case. Copied from fig. 5 in Rutledge et al. (1988).

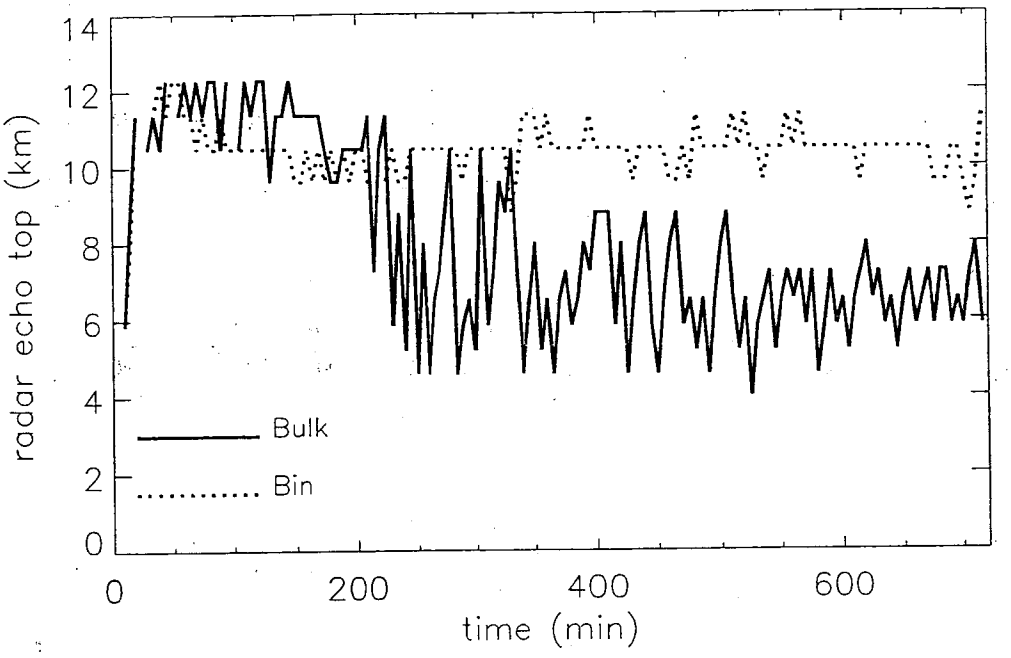

Figure 3: Time series of 30 dBZ radar echo top of the leading convective cell in the bulk (solid line) and bin (dashed line) simulations.

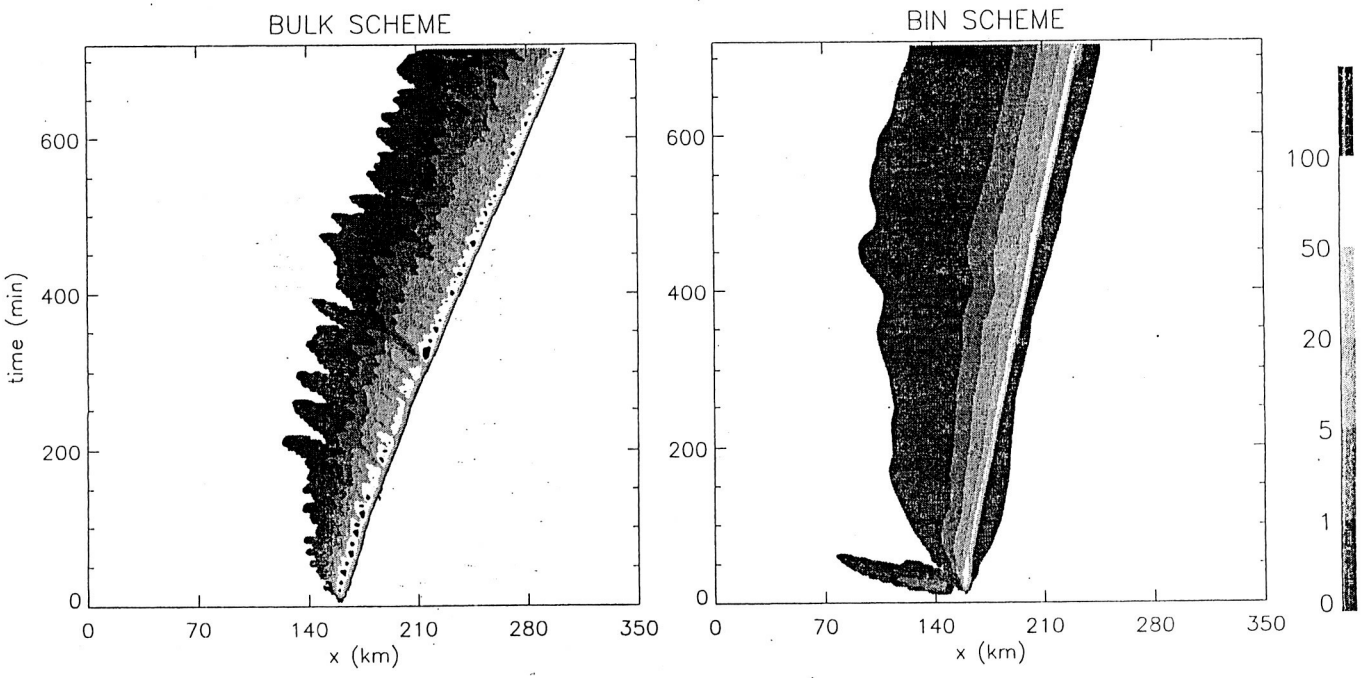

Figure 4: Time-domain diagram of surface rainfall for the bulk (4a) and bin (4b) schemes.

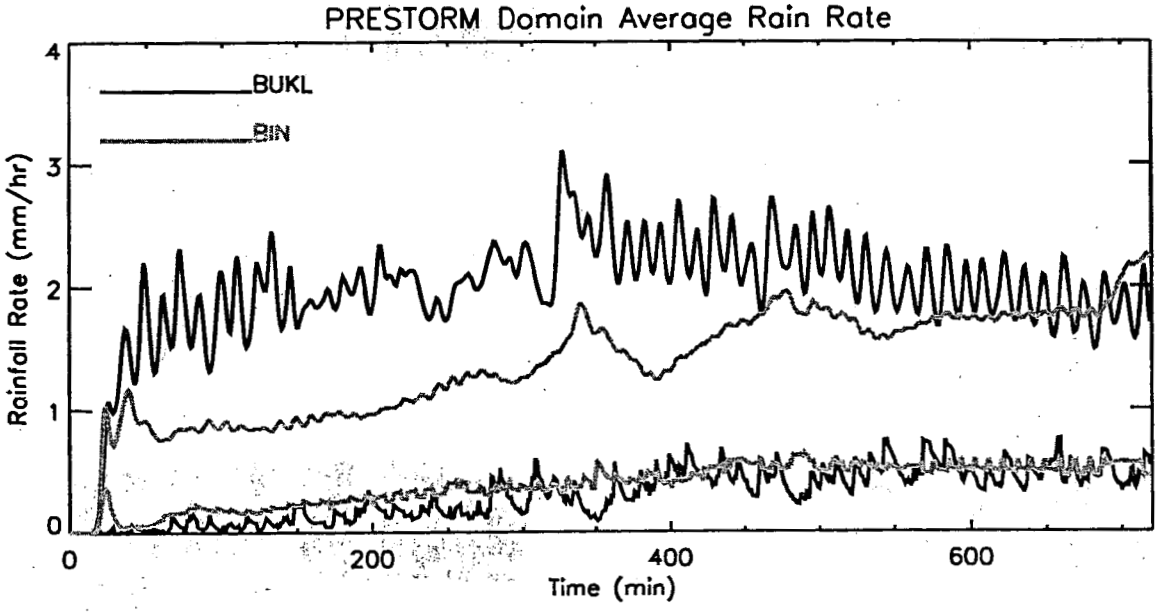

Figure 5: Time series of the domain average surface rainfall rate for the bulk (black lines) and bin (gray lines) simulations. The upper two lines are total surface rainfall rate, and lower two lines are stratiform rainrate using the CH_84 separation method.

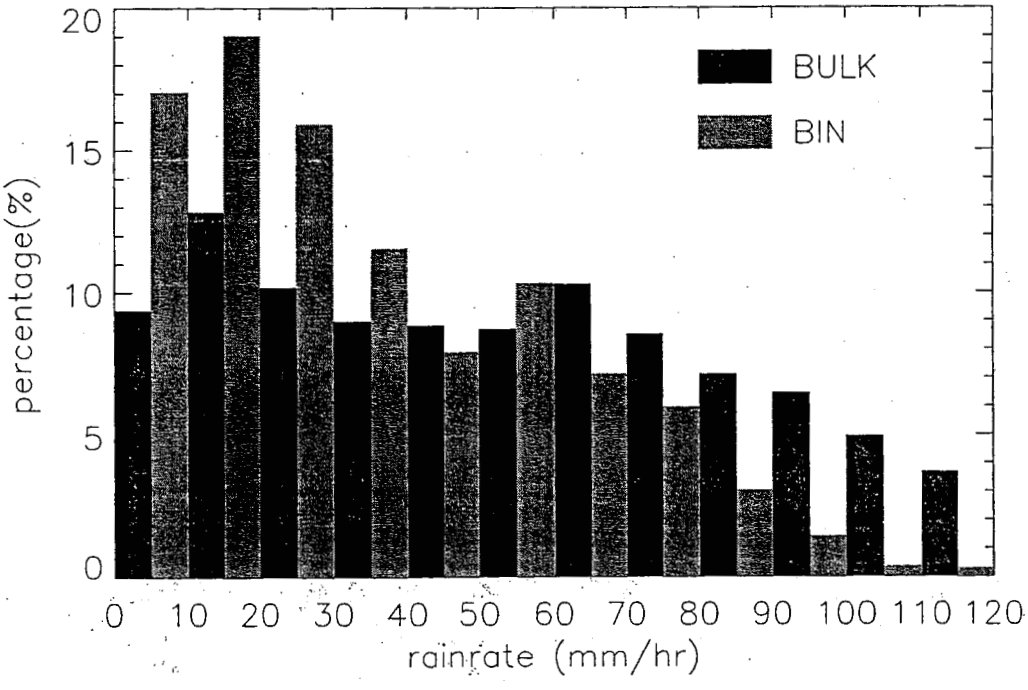

Figure 6: Surface rainfall amount probability density plot for the June 10-11 PRE-STORM case.

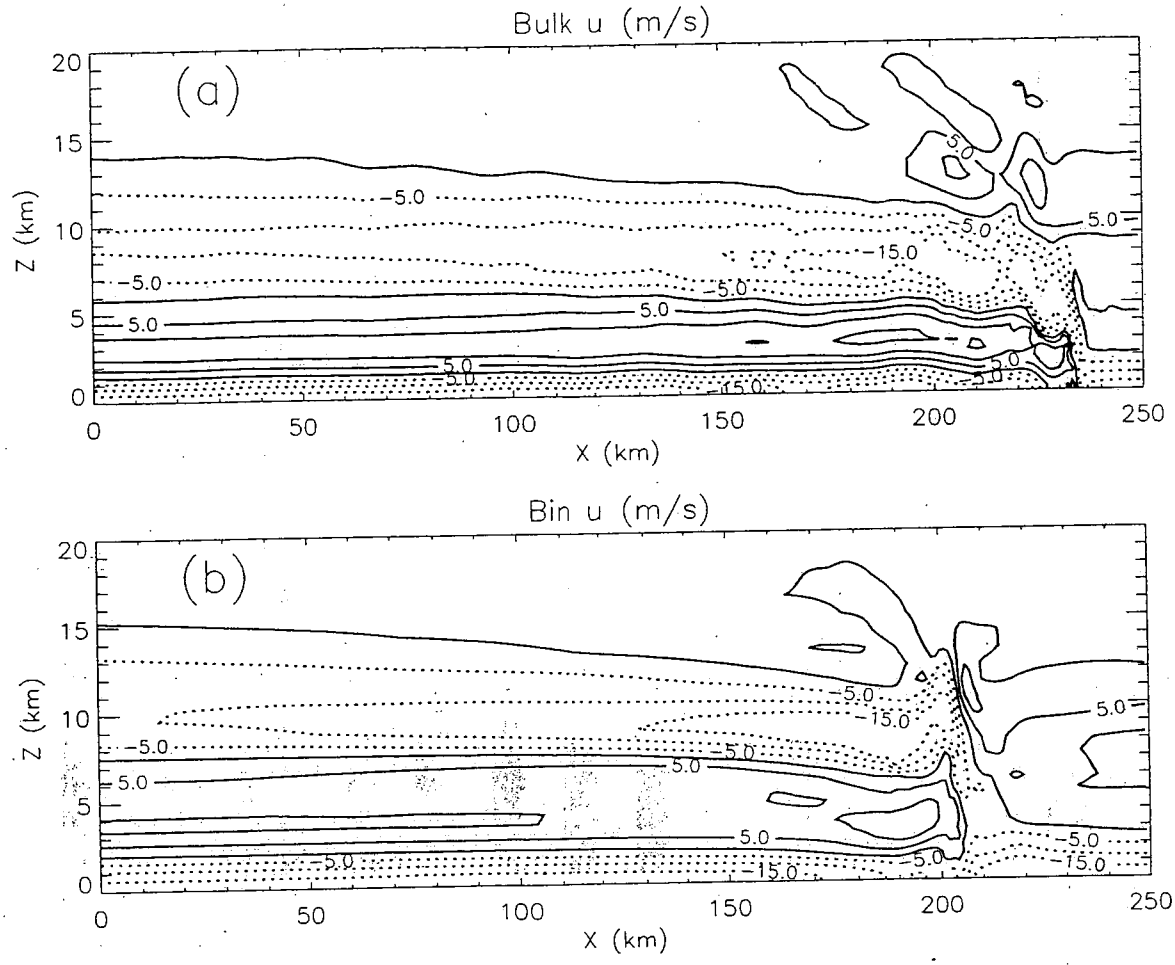

Figure 7: Horizontal wind field at the end of the simulation (12 hours) for bulk (7a) and bin (7b) scheme. Contour levels are -15, 10, -5, 0, 5, 10, 15m s^{-1}, with negative contours shown in dashed lines.

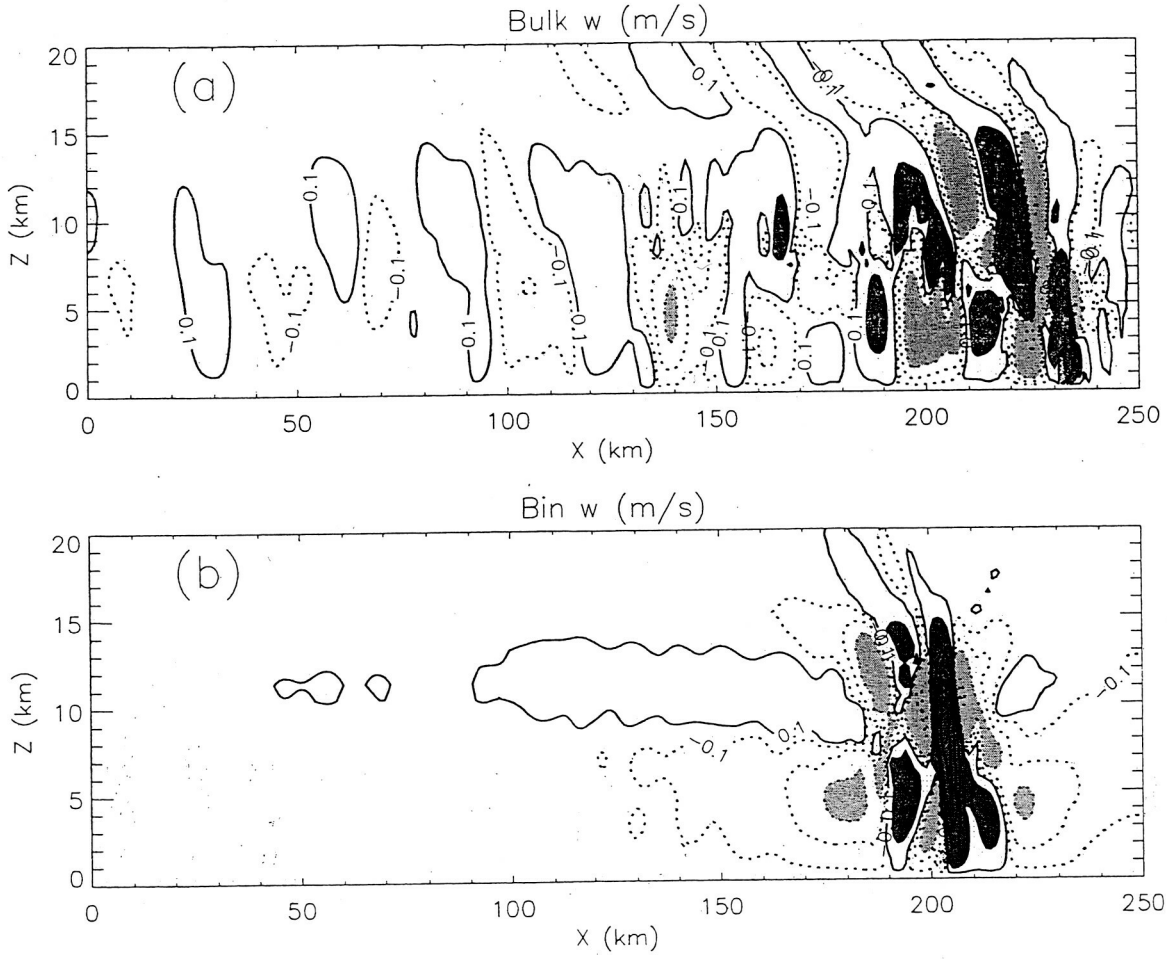

Figure 8: Vertical air velocity field after 12 hours of simulation for the bulk (8a) and bin (8b) scheme. Contour levels are –5, –1, -0.5, -0.1, 0.1, 1, 5, 10, and 20 m s^{-1}, with negative contours shown in dashed lines. Updraft cores with *w* bigger than 1 m s^{-1} are darkly shaded. Downdraft cores with *w* less than –1 m s^{-1} are lightly shaded.

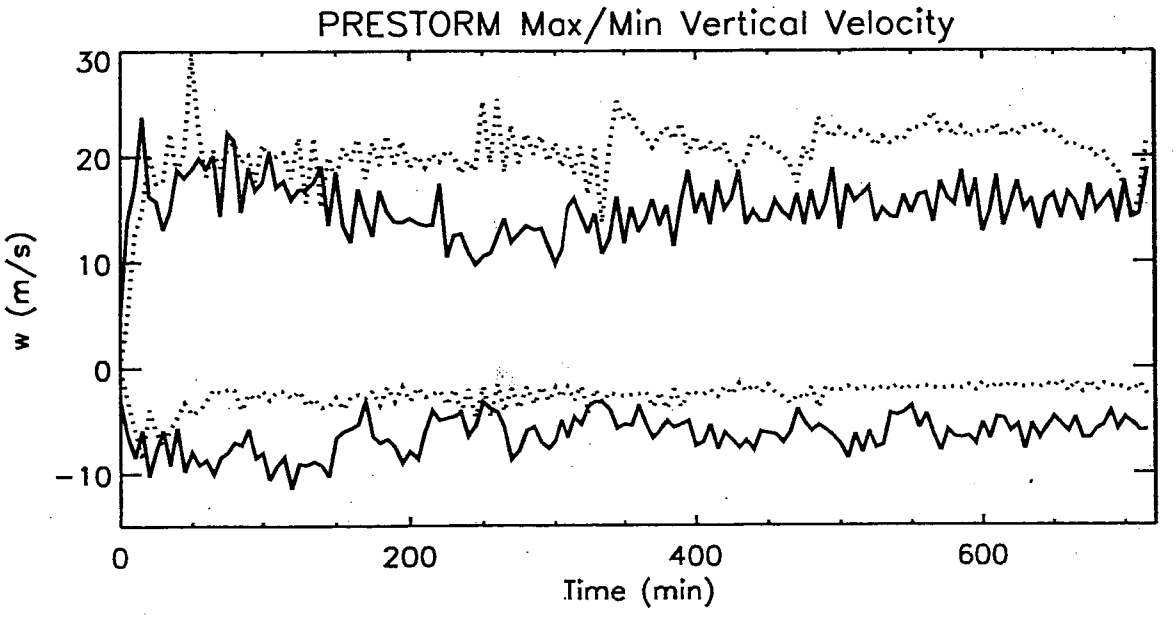

Figure 9: Time series of maximum and minimum vertical air velocity (m s^{-1}) for both the bulk (solid lines) and bin (dotted lines) simulations. Negative values represent downdrafts. The minimum velocity is calculated using only data below 5 km.

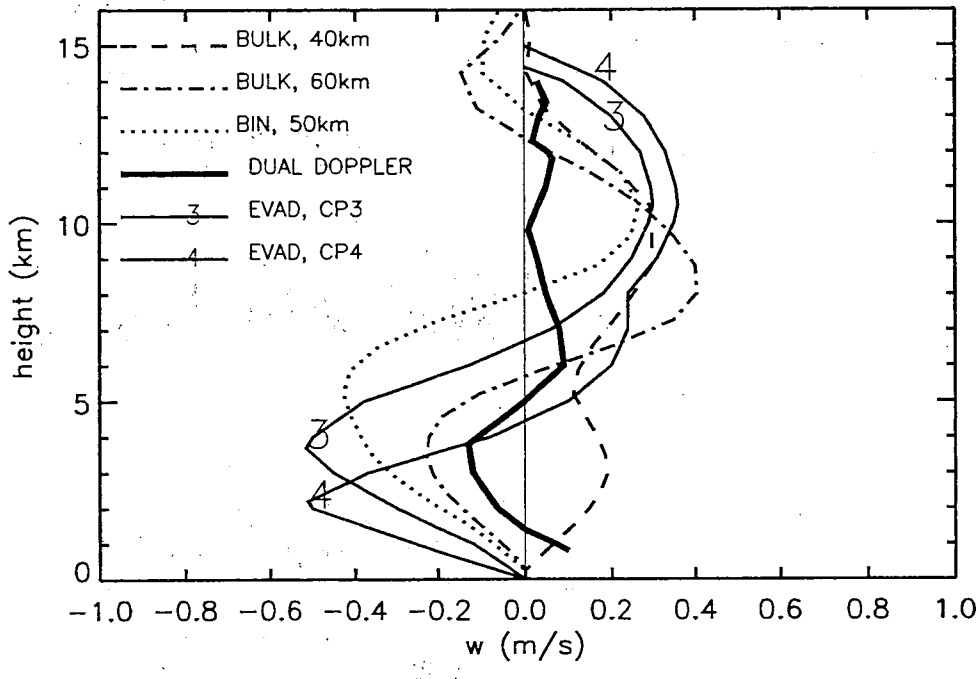

Figure 10: Average vertical air velocity profiles for the stratiform region 12 hours into the simulation. The dotted line is for the bin simulation averaged between x=130 km and 180 km in fig. 8b. The dashed line is for the bulk simulation averaged between x=150 km and 190 km in fig. 8a; The dashed-dot line is for the bulk simulation averaged between x=150 km and 210 km in fig. 8a. Thin solid lines are from EVAD calculations of the same case using CP3 and CP4 radar (Rutledge et al. 1988), and the thick solid line is the dual doppler radar estimation (Biggerstaff and Houze 1993).

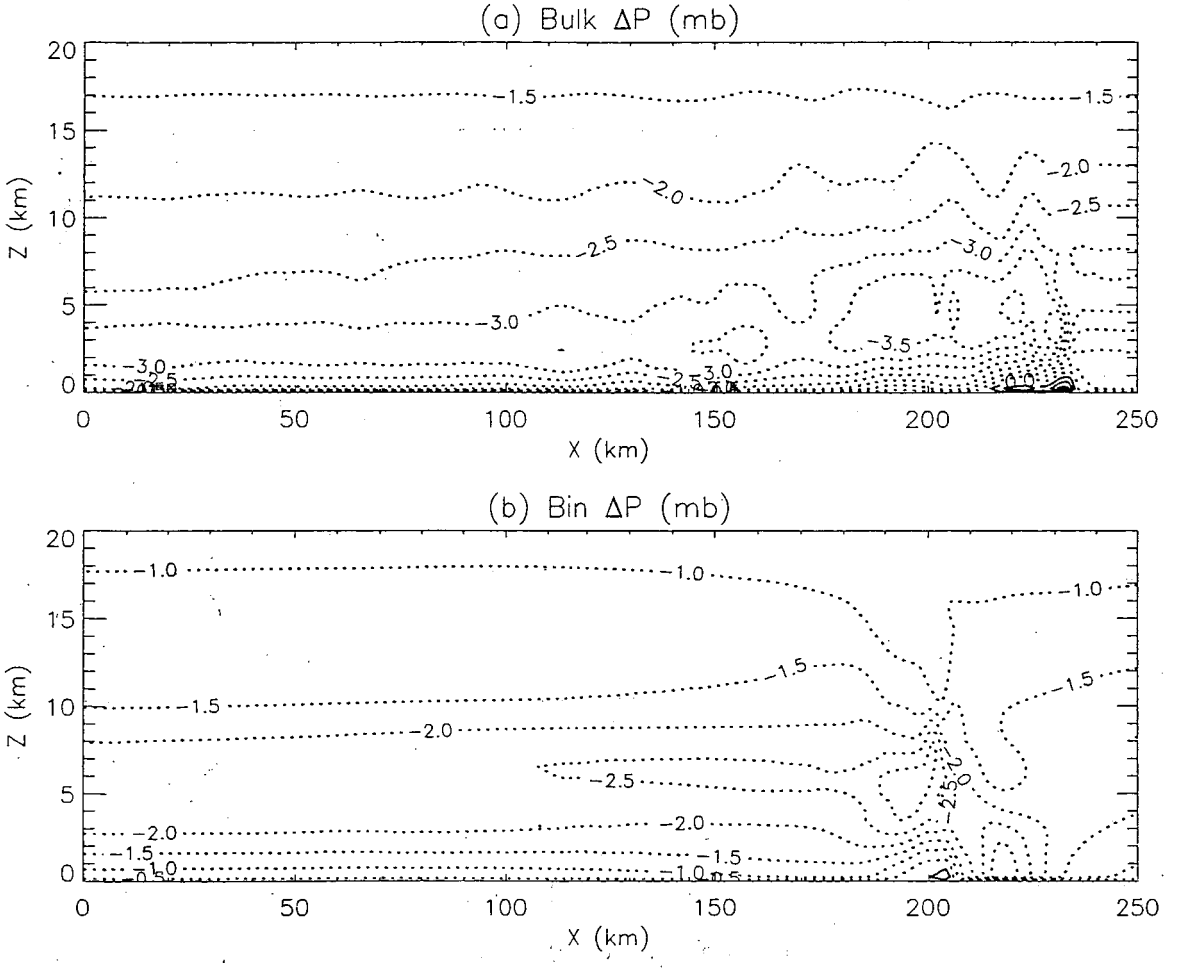

Figure 11: Pressure perturbations in the unit of mb for both bulk and bin simulations. Positive/negative values are in solid/dashed lines. The interval of the contours is 0.5 mb.

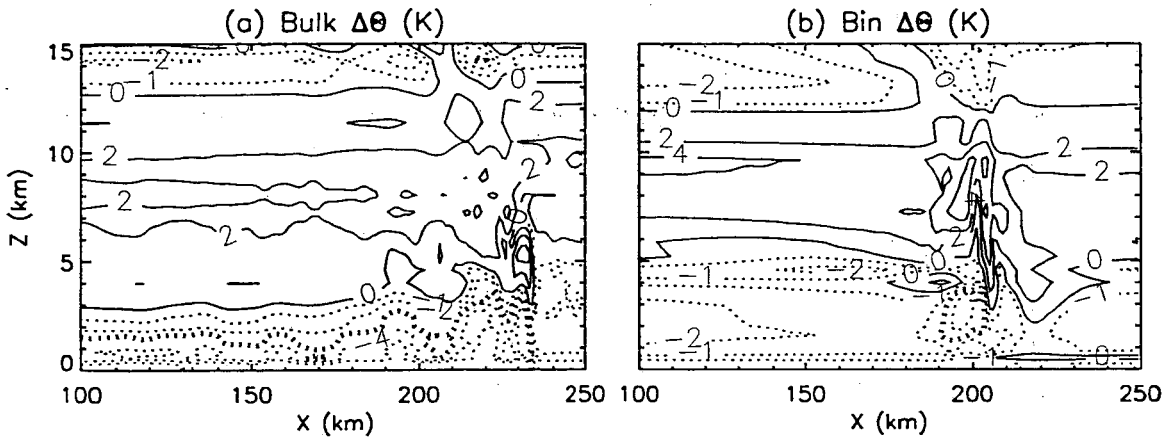

Figure 12: Potential temperature perturbation fields at t=12 hours for the bulk (12a) and bin (12b) models. Contour levels are –5 –4, -3, -2, -1, 0, 2, 4, 6 K, with negative contours in dashed lines. –3 K lines are marked with thick dashed lines.

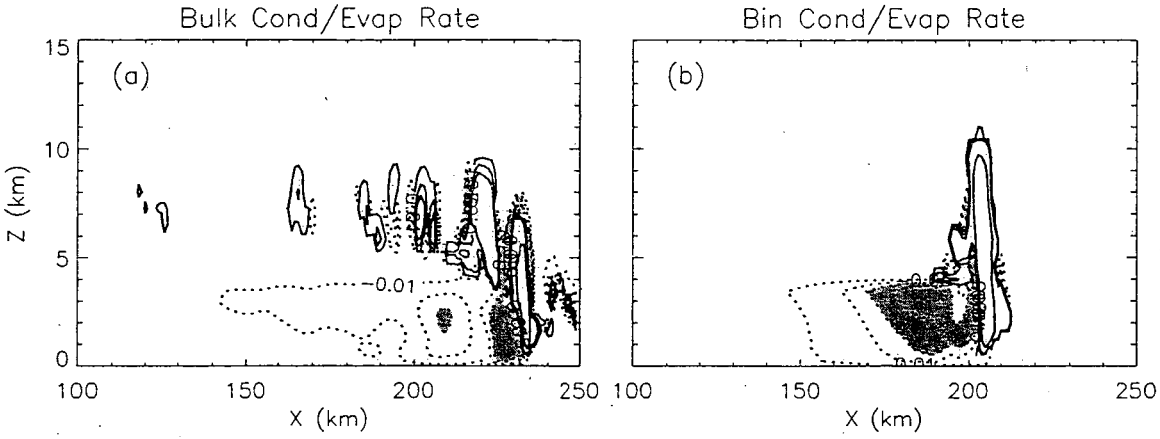

Figure 13: Condensation/evaporation rate field in g g^{-1} day^{-1} for the bulk (13a) and bin (13b) simulations. Positive values (condensation) are in solid lines, and negative values (evaporation) are in dashed lines. Contour levels are –0.2, -0.1, -0.05, -0.01, 0.01, 0.05, 0.1, 1.0 g g^{-1} day^{-1}. Areas with evaporation rates stronger than –0.1 g g^{-1} day^{-1} are shaded in gray.

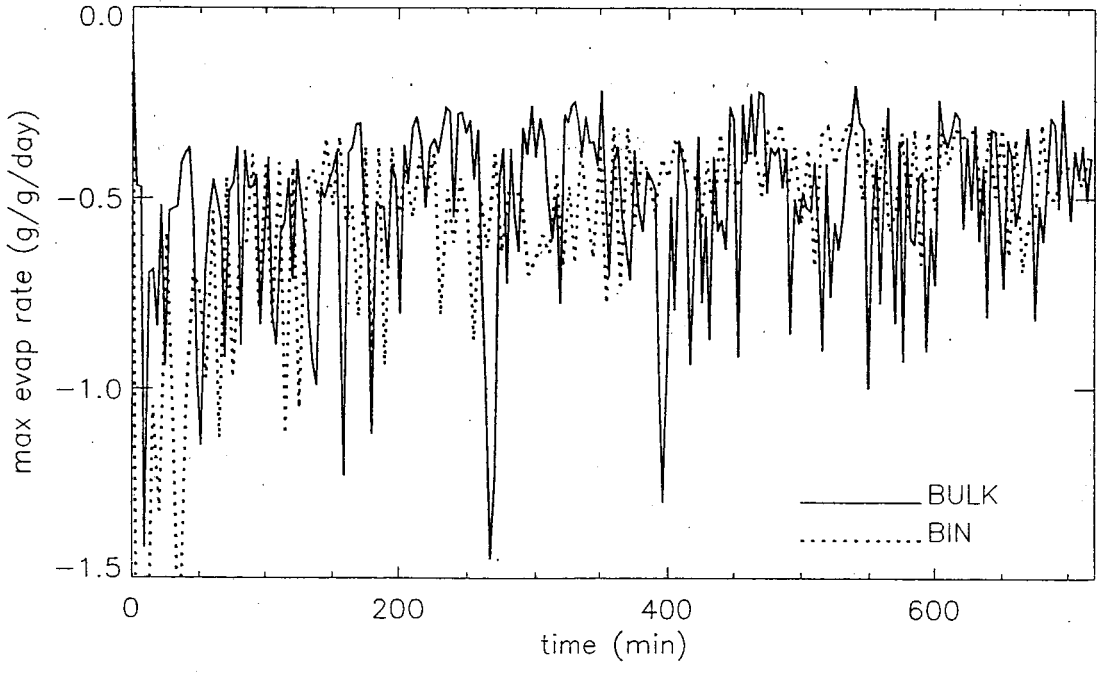

Figure 14: Time series of the maximum evaporation rate in g g^{-1} day^{-1}. Only evaporation rates below melting the level are used. The solid (dashed) line is the bulk (bin) simulation.

Popular Summary

Submitted as an article to *Journal of the Atmospheric Sciences*, June 2004.

Title: Sensitivity of a Cloud-Resolving Model to the Bulk and Explicit Bin Microphysical Schemes. Part I: Validations with a PRE-STORM Case

Authors: Xiaowen Li[1], Wei-Kuo Tao[2], Alexander P. Khain[3], Joanne Simpson[2], and Daniel E. Johnson[1]

The Goddard Cumulus Ensemble Model (GCE) is used to study sensitivities of two different microphysical schemes, one is the bulk type, and the other is an explicit bin scheme, in simulating a mid-latitude squall line case (PRE-STORM, June 10-11, 1985). Simulations using different microphysical schemes are compared with each other and also with the observations. Both the bulk and bin models reproduce the general features during the developing and mature stage of the system. The leading convective zone, the trailing stratiform region, the horizontal wind flow patterns, pressure perturbation associated with the storm dynamics, and the cool pool in front of the system all agree well with the observations. Both the observations and the bulk scheme simulation serve as validations for the newly incorporated bin scheme. However, it is also shown that the bulk and bin simulations have distinct differences, most notably in the stratiform region. Weak convective cells exist in the stratiform region in the bulk simulation, but not in the bin simulation. These weak convective cells in the stratiform region are remnants of the previous stronger convections at the leading edge of the system. The bin simulation, on the other hand, has a horizontally homogeneous stratiform cloud structure, which agrees better with the observations. Preliminary examinations of the downdraft core strength, the potential temperature perturbation, and the evaporative cooling rate show that the differences between the bulk and bin models are due mainly to the stronger low-level evaporative cooling in convective zone simulated in the bulk model.

[1] Goddard Earth Science and Technology Center, University of Maryland, Baltimore County
[2]Laboratory for Atmosphere, NASA Goddard Space Flight Center
[3]The Hebrew University of Jerusalem, Jerusalem, Israel